Journal of the Ceramic Society of Japan 120 [8] 311-316 2012 Paper

Obtainment of nanoparticulate CuNiZn ferrite powder by high-energy milling

Antonio BARBA,† Carolina CLAUSELL, Juan Carlos JARQUE and María MONZÓ

Instituto de Tecnología Cerámica, Asociación de Investigación de las Industrias Cerámicas, Universitat Jaume I, 12006 Castellón, Spain

This study was undertaken to obtain nanoparticulate CuNiZn ferrite powder by high-energy milling, as this is an approach that could potentially be scaled up for industrial use. Such nanometric particles may be expected to yield sintered ferrites with enhanced properties. The study was conducted using commercial pellets of CuNiZn ferrite powder as raw material. This was subjected to high-energy milling, producing ferrite nanoparticles with an average particle size of ~20 nm. These nanoparticles were then used to form test pieces that were sintered at 1100°C for 5 h, yielding high-density (96%) CuNiZn ferrite ceramics.

Key-words : CuNiZn ferrite, Nanoparticle, High-energy milling, Sintering

[Received March 28, 2012; Accepted June 6, 2012]

1. Introduction

The term ferrite was originally used for a class of mixed oxides with an inverse spinel structure with the general formula AFe_2O_4, A being a divalent metal ion. However, the term is often expanded to include other oxides that do not necessarily contain iron but have similar magnetic properties. Cu-doped NiZn ferrites are mainly used in manufacturing components for electric or electronic devices, owing to their ability to absorb electromagnetic radiation, thus avoiding interferences between different devices.[1)–4)] The electromagnetic properties of these materials are not just determined by their chemical composition, but also by their microstructure, such as the total porosity of the material, pore-size distribution, grain-size distribution, and grain boundary characteristics.[5)]

Numerous studies have shown that the mechanical and/or physical properties of ceramic bodies improve when particle-size distribution decreases from the microscale to the nanoscale.[6)–8)] In the last few decades, most research has focused on developing methods to obtain nanosized particles, particularly involving top-down methods (breaking down a bulk material into ever smaller particles), such as high-energy milling[9),10)] and mechanosynthesis,[11)–13)] and bottom-up methods (molecular self-assembly, arranging atoms or molecules into a desired pattern), such as sol–gel,[14),15)] chemical vapour deposition (CVD),[16)] physical vapour deposition (PVD), arc discharge,[17),18)] and laser ablation.[19)]

Most of these methods have also been used in recent years to obtain nanosized NiZn ferrite powders. Such methods include chemical co-precipitation,[20)–23)] mechanochemical synthesis,[24)–28)] combustion reaction,[29)–33)] hydrolysis,[34)] high-energy ball milling,[35)–37)] low-temperature synthesis,[38)] and the sol–gel process.[39),40)]

As a follow-up to the authors' previous work on the sintering[41)–47)] and properties[48)] of ceramic materials obtained from micrometric Cu-doped NiZn ferrite particles, the present study was undertaken to obtain nanometric CuNiZn ferrite particles using a high-energy milling process. The principal advantage of this approach is that it is a method that could potentially be scaled up to an industrial scale, as it enables large quantities of nanoparticulate powders to be prepared at ambient temperature, using cheap raw materials and relatively economical facilities, while being a relatively simple method. Such nanometric particles may be expected to yield sintered ferrites with enhanced properties.

In this study, a nanoparticulate CuNiZn ferrite powder was prepared by high-energy milling and used to form test pieces by uniaxial dry pressing. These pieces were subsequently sintered using infrared radiation. The resulting high-density pieces were microstructurally characterised and the results obtained were compared with those of pieces formed from micrometric particles of the same chemical composition.

2. Material and methods

A CuNiZn ferrite powder, supplied as pellets by Fair-Rite Products Corp., was used as raw material. The true density of the ferrite powder was experimentally determined on a helium pycnometer to be 5380 kg/m^3.

The pellets were milled for 2 h in a FRITSCH Pulverisette 5 planetary ball mill, where a rotating disk carries vials that rotate in opposite directions. Disk rotation speed was 260 rpm and milling was done in carbon steel vials, using carbon steel balls, 7–8 mm in diameter. The resulting milled powder (referenced 0h) exhibited a micrometric particle size distribution.

The powder was then wet milled in a VMA-GETZMANN Dispermat SL-012 laboratory horizontal bead mill. The mill has a 125-ml capacity milling chamber and runs at a maximum speed of 6000 rpm and 1.1 kW power. Milling was performed using distilled water and zirconia beads, 0.5–0.7 mm in diameter. A 3 wt% ammonium polymethacrylate solution (DARVAN® C, RT Vanderbilt Company Inc.), to dry solid, was used as dispersant agent. Milling speed was 4500 rpm; this was kept constant in all experiments. The bead-to-ferrite powder volume ratio was 3:2 and milling times ranged from 0.5 to 48 h.

The powder obtained after each milling time was dried and sieved. Particle/agglomerate-size distribution was determined by laser light diffraction (LLD) (wet method) using a MALVERN Mastersizer 2000 particle size analyser. A powder suspension

† Corresponding author: A. Barba; E-mail: barba@qui.uji.es

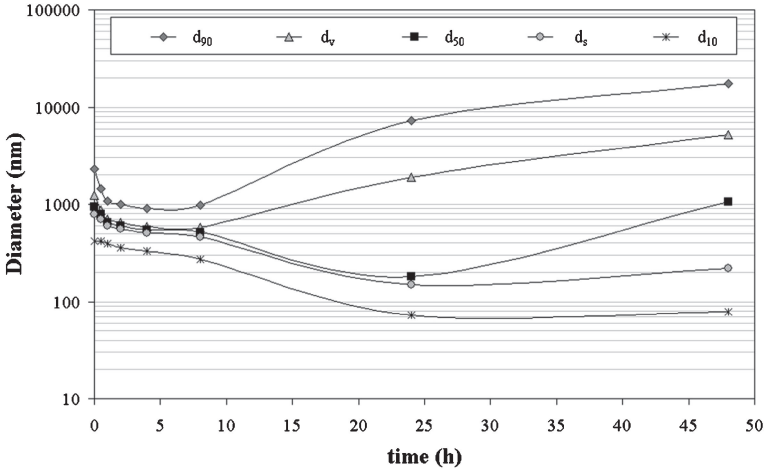

Fig. 1. Equivalent diameters obtained from particle/agglomerate-size distributions determined by laser light diffraction (LLD) at different milling times (0, 0.5, 1, 2, 4, 8, 24, and 48 h).

was prepared using an aqueous solution of ammonium polymethacrylate, Darvan® C (1 kg/m^3). The suspension was treated by ultrasonic waves for 5 min and stored for 24 h in order to wholly disperse the particles. The suspension was then treated again by ultrasonic waves for 5 min, followed by mechanical stirring, before determining the particle/agglomerate-size distribution. The Mie theory was used to analyse the light dispersed by the suspension: the Fe_2O_3 refractive index was assumed to be 2.94 and the absorption coefficient to be 0.01. The data were processed using the software supplied with the equipment. The following parameters were determined, assuming spherical particles/agglomerates: d_{90}, d_{50} and d_{10} equivalent diameters, average bulk diameter (d_V) and average surface diameter (d_S).

The BET specific surface area (S_{BET}) was determined by nitrogen adsorption on a MICROMERITICS TriStar 3000 instrument. After milling, the resulting ferrite powder suspension was dried at 110°C for 2 h. The powder obtained was degasified in a nitrogen stream at 150°C. The quantity of adsorbed nitrogen was then determined by a static volumetric method. An average equivalent spherical particle diameter (D_{BET}) was calculated for each milling time, tested by the equation[49] $D_{BET} = 6/(\rho_t \cdot S_{BET})$, where ρ_t is ferrite true density.

Crystallite size was analysed by X-ray diffraction (XRD) in a BRUKER D8 Advance diffractometer. The XRD tests were conducted using following measurement conditions: Cu tube; divergence and receiving slit widths, 0.6 mm; voltage, 30 kV; intensity, 40 mA; without monochromator; time constant, 0.5 s; and 2θ range of 5 to 90°. Crystallite size was determined using the 4.2 version of the Rietveld analysis program, DIFFRACplus TOPAS, assuming a pseudo-Voight function to describe peak shapes.[50]

Morphological analysis was performed by scanning electron microscopy (SEM) using a FEI Quanta 200 ESEM FEG microscope. For the SEM analyses, samples were sputter coated with platinum (Balzers SDC 040) using a current of 20–22 mA for 20 s.

The resulting powders were used to form test pieces by uniaxial dry pressing at 200 MPa. These pieces were sintered at 1100°C for 5 h. Test piece dry and sintered bulk density was determined by the Archimedes method. The relative density (ϕ) of each ferrite specimen was calculated as the quotient of bulk density to true density. Grain-size distribution was determined by image analysis of the SEM micrographs taken at the surface of cross-sections of polished and thermally attacked ferrite pieces.

3. Results and discussion

The particles in a nanosized powder are the result of the chemical aggregation of a number of crystallites with different crystal orientations, which means that the crystallites can be observed by XRD. It may be noted that, in some papers, the term 'aggregate' is also used to describe the physical aggregation of particles when they are not well dispersed. The term 'aggregates' in the scientific literature tends to be confusing, and sometimes particle size and crystallite size are even used as synonyms. In this paper, the term 'aggregate' is used to define a set of particles held together by a strong chemical bond, while the term 'agglomerate' is used to define a set of particles held together by a weak physical bond.

In this study, crystallite size was determined by XRD, while particle size was determined by the BET specific surface area. Laser light diffraction (LLD) was also evaluated, as LLD is customarily used to determine particle/agglomerate size (resulting from the physical agglomeration of particles). The difference between the XRD and BET determinations provides a measure of the degree of chemical aggregation of the crystallites.[51),52] However, only the value of particle size is useful in processing nanopowders.

3.1 Characterisation of the milled ferrites

The evolution of equivalent diameters d_{90}, d_{50}, d_{10}, d_V, and d_S versus milling time is shown in **Fig. 1**. The results of the 0 h sample correspond to the ferrite sample of micrometre-sized particles, subsequently used in the sintering study. In the first 4 h of milling, the average particle/agglomerate size (d_{50}) decreased from 940 to 550 nm, and the width of the particle/agglomerate-size distribution (calculated as d_{90}–d_{10}) also decreased from 1870 to 570 nm. However, when milling time exceeded four hours, d_{90} and d_v increased. After 24 h of milling, d_{50} was observed to increase. Finally, after 48 h of milling, d_S and d_{10} increased.

The results obtained by LLD suggest that an agglomeration process occurred during milling in the ferrite powder suspension. The agglomeration process was probably caused by an increase in ferrite particle surface energy and by the occurrence of structural crystalline imperfections when the powder was mechanically milled.[51),52] In other words, the coordination number of

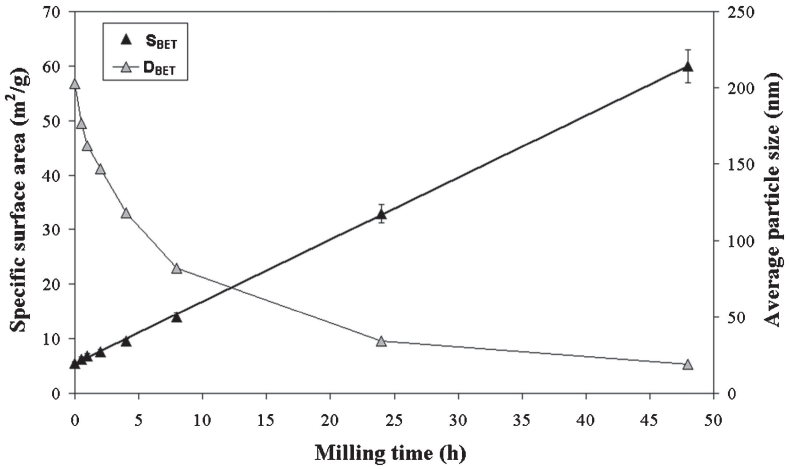

Fig. 2. Specific surface area (S_{BET}) and average particle size (D_{BET}) determined by BET at different milling times (0, 0.5, 1, 2, 4, 8, 24, and 48 h).

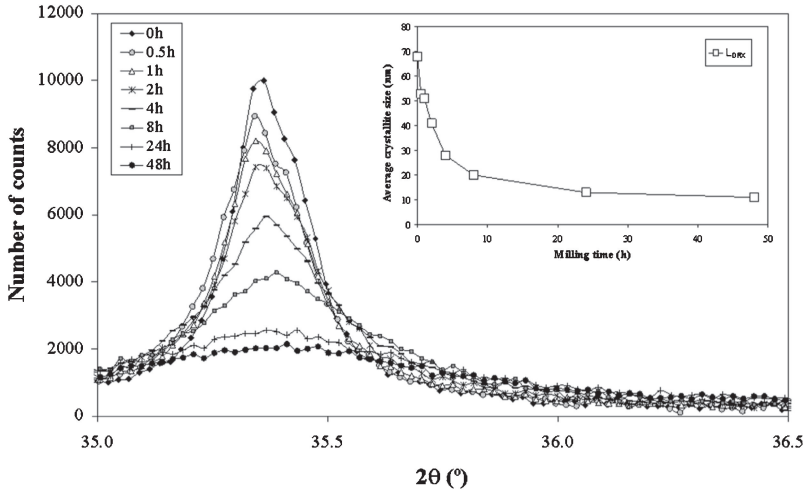

Fig. 3. Maximum intensity peak of X-ray powder diffraction profiles at different milling times (0, 0.5, 1, 2, 4, 8, 24, and 48 h), corresponding to the $Zn(Fe_2O_4)$ crystal structure, and average crystallite size vs. milling time determined by DRX (L_{DRX}).

particle surface atoms decreased during milling, causing excess surface polarisation, which activated the surfaces and increased their reactivity, leading to particle agglomeration.[51),52)] Attraction magnetic forces also play an important role in ferrites.

The LLD technique was, thus, found to be unsatisfactory for determining the particle-size distribution of nickel–zinc ferrite nanopowders because, in fact, agglomerate-size distribution was being determined.

The evolution of the specific surface area (S_{BET}) versus milling time is shown in **Fig. 2**. S_{BET} increased linearly with milling time and ranged from 5.5 to 60 m^2/g, according to the following empirical equation: $S_{BET} = 1.138 \cdot t + 5.403$, where t is milling time (h). The values of the average particle size (D_{BET}) (grey triangles) are also included in Fig. 2. As may be observed, D_{BET} decreased with milling time, ranging from 203 nm at 0 h to 19 nm at 48 h. A sharp decrease occurred during the first four hours of milling, followed by a gentle decrease at longer milling times.

The $Zn(Fe_2O_4)$ ferrite was the only crystalline structure identified in all tested samples. **Figure 3** shows the ferrite maximum intensity peak at different milling times and the evolution of average crystallite size vs. milling time. It may be observed that peak intensity decreased with milling time from 9994 counts at 0 h to 2139 counts at 48 h, reflecting a progressive decrease in crystallite size from 68 to 11 nm (white squares in Fig. 3 corner).

The evolution of agglomerate/particle/crystallite size is plotted in **Fig. 4** as a function of milling time, determined by LLD (●), BET (▲), and XRD (□), respectively. These results indicate that the Ni–Zn ferrite nanoparticles probably displayed some degree of chemical aggregation of the crystallites, because crystallite size was always smaller than particle size.[51),52)] Crystallite size and particle size both decreased with high-energy milling, while the average number of crystallites aggregated per particle also dropped from 4 to 2.

Figure 5 shows SEM micrographs of three powder samples obtained at three different test milling times (8, 24, and 48 h), taken at a final magnification of 300000×. The micrographs show that the particle sizes match the average particle sizes determined by the BET specific surface area (D_{BET}). In the case of the sample milled for 48 h, the resulting particle size was about 25–30 nm.

3.2 Characterisation of the sintered pieces

Figure 6 shows SEM micrographs of: (a) the microparticulate ferrite powder sample at 0 h; (b) the nanoparticulate ferrite powder corresponding to the sample at 48 h; and polished and

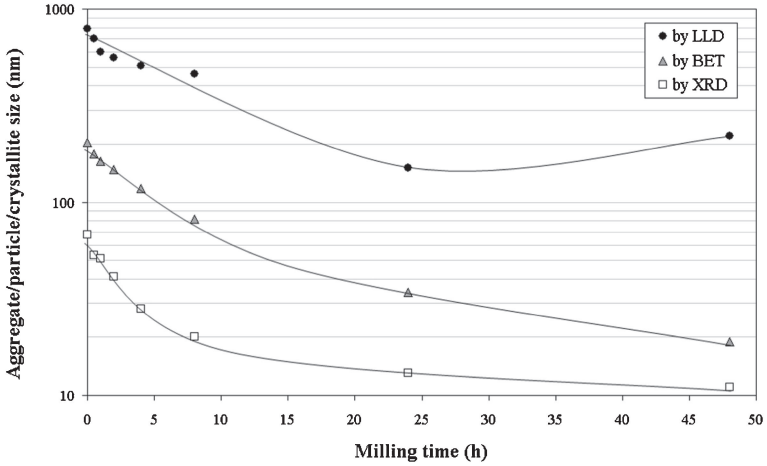

Fig. 4. Agglomerate size vs. milling time determined by LLD (●), particle size vs. milling time determined by BET (▲), and crystallite size vs. milling time determined by XRD (□).

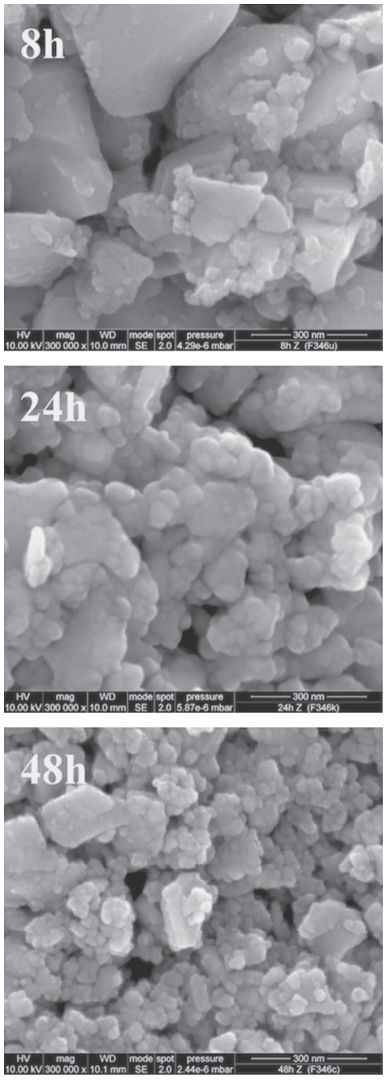

Fig. 5. SEM micrographs taken at different milling times (8, 24, and 48 h).

thermally attacked cross-sectional surfaces of sintered pieces obtained from the (c) microparticulate and (d) nanoparticulate ferrite powder. The sintered pieces are observed to exhibit a homogeneous grain-size distribution, without exaggerated growth of isolated grains.

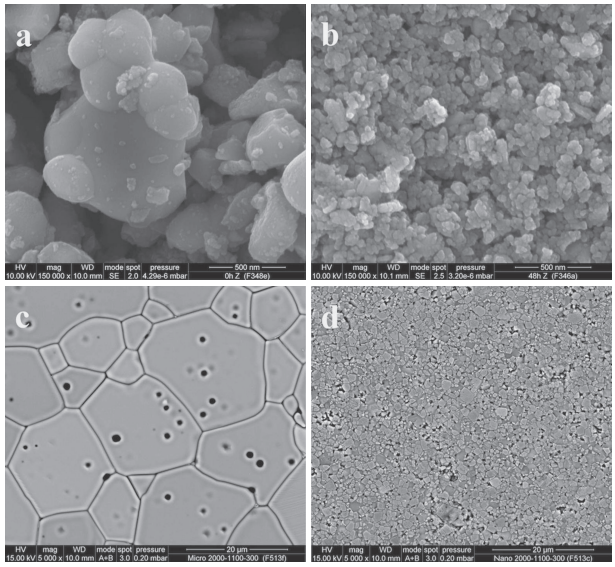

Fig. 6. SEM micrographs of the (a) microparticulate and (b) nanoparticulate ferrite powders and of the corresponding sintered pieces: (c) obtained using the microparticulate ferrite powder and (d) obtained using the nanoparticulate ferrite powder.

Table 1. Relative density and characteristic grain diameters of the sintered pieces obtained with the micrometric and nanometric ferrite particles

Sample	ϕ_c	d_{10} (μm)	d_{50} (μm)	d_{90} (μm)
Micrometric ferrite particles	0.957	8.91	16.94	29.63
Nanometric ferrite particles	0.960	0.45	0.95	1.60

The relative density of the sintered pieces obtained from the micrometric and the nanometric ferrite particles (0.960 and 0.957, respectively), as well as the characteristic grain diameters d_{10}, d_{50}, and d_{90}, determined by image analysis of the SEM micrographs of both sintered pieces, are detailed in **Table 1**.

The results in Table 1 indicate that the nanometric ferrite particles yielded sintered pieces with high relative density (similar to that produced using micrometric ferrite particles).

However, the average grain size and width of the grain-size distribution decreased considerably, from a d_{50} of 16.94 μm for the piece obtained using the micrometric particles to a d_{50} of 0.95 μm for the piece obtained using the nanometric particles.

According to the literature,[6)–8)] the reduction in average grain size and the narrowing of the width of the resulting grain-size distribution, when nanometric ferrite particles are used, should significantly improve the final properties of this type of ferrite.

4. Conclusions

In this study, nanometric particles of a Cu-doped Ni–Zn ferrite were obtained by high-energy milling, a process that could potentially be scaled up for industrial use. The particle comminution process was monitored by various techniques: laser light diffraction (LLD), nitrogen adsorption (BET), X-ray diffraction (XRD), and scanning electron microscopy (SEM).

The LLD technique was shown to be inappropriate for the determination of the nanometric particle sizes of this type of material because agglomeration of the material occurred during sample preparation (owing to the high surface energy of these particles and, in the case of ferrites, as a result of the attraction forces present in the material). In contrast, the BET technique proved to be appropriate for the determination of particle sizes of this type of ferrite. The XRD technique allowed the crystallite size to be determined.

Sintered pieces with high relative density were obtained from the studied nanometric ferrite particles. Their relative density was similar to that of sintered pieces obtained from micrometric ferrite particles of the same composition, but the grain-size distribution was much finer and narrower: an average grain size of about 1 micrometre was obtained, compared with the 17 micrometres obtained when micrometric ferrite particles were used. The use of nanometric ferrite particles may be expected to enhance many of the physical properties of the resulting sintered ferrites.

Acknowledgments The study was conducted with funding from the MAT2008-05590 project in the 6th Spanish National Plan for Scientific Research, Development, and Technology Innovation 2008–2011.

References

1) K. Y. Kim, W. S. Kim, Y. D. Ju and H. J. Jung, *J. Mater. Sci.*, 27, 4741–4745 (1992).
2) W. S. Kim, S. J. Yoon and K. Y. Kim, *Mater. Lett.*, 19, 149–155 (1994).
3) S. R. Murthy, *J. Mater. Sci. Lett.*, 21, 657–660 (2002).
4) J. Kulikowski and A. Lesniewski, *J. Magn. Magn. Mater.*, 19, 117–119 (1980).
5) Z. Lan, Z. Yu and J. Wang, *J. Funct. Mater.*, 5, 486–487 (2000).
6) M. Y. Tian, E. W. Shi, W. Z. Zhong, W. Q. Pang and J. K. Guo, *J. Inorg. Mater.*, 13, 129–137 (1998).
7) T. P. Comyn, D. F. Kanguwe, J. Y. He and A. P. Brown, *J. Eur. Ceram. Soc.*, 28, 2233–2238 (2008).
8) M. Lebedev, J. Akedo and A. Iwata, *J. Am. Ceram. Soc.*, 87, 1621–1624 (2004).
9) N. Kislov, S. S. Srinivasan, Y. Emirov and E. K. Stefanakos, *Mater. Sci. Eng.*, 153, 70–77 (2008).
10) A. Narayanasamy and N. Sivakumar, *Bull. Mater. Sci.*, 31, 373–380 (2008).
11) M. Sinha, H. Dutta and S. K. Pradhan, *Jpn. J. Appl. Phys.*, 47, 8667–8672 (2008).
12) M. J. S. Isfahani, M. Myndyk, D. Menzel, A. Feldhoff, J. Amighian and V. Šepelák, *J. Magn. Magn. Mater.*, 321, 152–156 (2009).
13) M. J. S. Isfahani, M. Myndyk, V. Šepelák and J. Amighian, *J. Alloys Compd.*, 470, 434–437 (2009).
14) W. C. Kim, S. I. Park, S. J. Kim, S. W. Lee and C. S. Kim, *J. Appl. Phys.*, 87, 6241–6243 (2000).
15) W. C. Kim, S. J. Kim, Y. R. Uhm and C. S. Kim, *IEEE Trans. Magn.*, 37, 2362–2365 (2001).
16) M. Veith, *Mater. Sci. Forum*, 343–346, 531–538 (2000).
17) Y. I. Kim, E. Nishikawa and T. Kka, *J. Korean Phys. Soc.*, 54, 1032–1035 (2009).
18) G. Xing, S. L. Jia and Z. Q. Shi, *New Carbon Mater.*, 22, 337–341 (2007).
19) T. Tsuji, M. Nakanishi, T. Mizuki, M. Tsuji, T. Doi, T. Yahiro and J. Yamaki, *Appl. Surf. Sci.*, 255, 9626–9629 (2009).
20) G. S. Shahane, A. Kumar, M. Arora, R. P. Pant and K. Lal, *J. Magn. Magn. Mater.*, 322, 1015–1019 (2010).
21) S. Modak, M. Ammar, F. Mazaleyrat, S. Das and P. K. Chakrabarti, *J. Alloys Compd.*, 473, 15–19 (2009).
22) W. C. Hsu, S. C. Chen, P. C. Kuo, C. T. Lie and W. S. Tsai, *Mater. Sci. Eng., B*, 1111, 142–149 (2004).
23) B. P. Rao, A. M. Kumar, K. H. Rao, Y. L. N. Murthy, O. F. Caltun, I. Dumitru and L. Spinu, *J. Optoelectron. Adv. Mater.*, 8, 1703–1705 (2006).
24) M. Jalaly, M. H. Enayati, F. Karimzadeh and P. Kameli, *Powder Technol.*, 193, 150–153 (2009).
25) M. Jalaly, M. H. Enayati, P. Kameli and F. Karimzadeh, *Physica B*, 405, 507–512 (2010).
26) S. Bid and S. K. Pradhan, *Mater. Chem. Phys.*, 84, 291–301 (2004).
27) Y. Lu, J. Zhang, Y. Liu, C. Jing and S. Cao, *J. Magn. Magn. Mater.*, 288, 54–59 (2005).
28) J. S. Jiang, L. Gao, X. L. Yang, J. K. Guo and H. L. Shen, *J. Mater. Sci. Lett.*, 18, 1781–1783 (1999).
29) P. Priyadharsini, A. Pradeep, P. Sambasiva Rao and G. Chandrasekaran, *Mater. Chem. Phys.*, 116, 207–213 (2009).
30) P. Priyadharsini, A. Pradeep and G. Chandrasekaran, *J. Magn. Magn. Mater.*, 321, 1898–1903 (2009).
31) S. Deka and P. A. Joy, *Mater. Chem. Phys.*, 100, 98–101 (2006).
32) A. C. F. M. Costa, E. Tortella, E. Fagury Netob, M. R. Morelli and R. H. G. A. Kiminamib, *Mater. Res.*, 7, 523–528 (2004).
33) A. C. F. M. Costa, E. Tortella, M. R. Morelli and R. H. G. A. Kiminami, *CFI, Ceram. Forum Int.*, 79, E34–E38 (2002).
34) Z. Beji, L. S. Smiri, N. Yaacoub, J. M. Grenèche, N. Menguy, S. Ammar and F. Fiévet, *Chem. Mater.*, 22, 1350–1366 (2010).
35) B. P. Rao, O. Caltun, W. S. Cho, C. O. Kim and G. G. Kim, *J. Magn. Magn. Mater.*, 310, e812–e814 (2007).
36) N. Sivakumar, A. Narayanasamy and N. Ponpandian, *J. Appl. Phys.*, 101, 084116 (2007).
37) B. P. Rao and O. F. Caltun, *J. Optoelectron. Adv. Mater.*, 8, 991–994 (2006).
38) S. Verma, S. D. Pradhan, R. Pasricha, S. R. Sainkar and P. A. Joy, *J. Am. Ceram. Soc.*, 88, 2597–2599 (2005).
39) B. P. Rao, Y. L. N. Murhty, S. M. Hong, C. O. Kim and G. G. Kim, *J. Appl. Phys.*, 101, 123902 (2007).
40) L. Q. Ling, Y. Yun, W. Y. Fei, J. Hong-Xia and W. Ya-Kun, "Key engineering materials (vol. 334–335) Advances in composite materials and structures", Ed. by J. K. Kim, et al., Trans Tech, Uetikon-Zuerich (2007) pp. 993–996.
41) A. Barba, C. Clausell, C. Felíu and M. Monzó, Proc. VIII Congreso Nacional de Materiales, Jun. 15–17, Valencia. Spain (2004) pp. 317–324.
42) A. Barba, C. Clausell, C. Felíu and M. Monzó, *J. Am. Ceram. Soc.*, 87, 571–577 (2004).
43) A. Barba, C. Clausell, M. Monzó and V. Cantavella, Proc. X Congreso Mediterráneo de Ingeniería Química: Ingeniería química y vida, Nov. 15–18, Barcelona, Spain (2005) pp. 185.
44) A. Barba, C. Clausell, M. Monzó and V. Cantavella, Proc. XLV reunión anual de la Sociedad Española de Cerámica y Vidrio, Nov. 2–5, Seville, Spain (2005).

45) C. Clausell, Sinterización en fase sólida de una ferrita de Cu, Ni, Zn: estudio de la cinética del proceso del desarrollo microestructural y de la permeabilidad magnética. PhD thesis. Castellón: Universitat Jaume I, Department of Chemical Engineering; 2008.
46) A. Barba, C. Clausell, M. Monzó and J. C. Jarque, *Bol. Soc. Esp. Ceram. Vidrio.*, **47**, 13–23 (2008).
47) A. Barba, C. Clausell, M. Monzó and J. C. Jarque, *Bol. Soc. Esp. Ceram. Vidrio.*, **47**, 101–104 (2008).
48) A. Barba, C. Clausell, C. Felíu, M. Monzó, L. Nuño, D. Heras and J. V. Balbastre, *J. Am. Ceram. Soc.*, **87**, 1314–1318 (2004).
49) R. C. Garvie, *J. Phys. Chem.*, **69**, 1238–1243 (1965).
50) R. A. Young, "The Rietveld method", Ed. by IUCr, Oxford University Press, New York (1993).
51) J. Carretero, M. A. Sainz, S. Serena and A. Caballero, *Bol. Soc. Esp. Ceram. Vidrio.*, **42**, 303–310 (2003).
52) J. C. Ray, P. Pramanik and S. Ram, *Mater. Lett.*, **48**, 281–291 (2001).